Adsorption Isotherms for CBY 3G-P Dye Removal from Aqueous Media Using TiO_2 Degussa, Fe_2O_3, and TiO_2/(DPC)

Shireen Abdulmohsin Azeez, Fadhela Muhammad Hussein, and Rasha Wali Mohi Al-Saedi*

Department of Chemistry, College of Science, Mustansiriyah University, Baghdad 10052, Iraq

* ***Corresponding author:***

email:
rwmal_saedi2@uomustansiriyah.edu.iq

Received: December 2, 2022
Accepted: March 7, 2023

DOI: 10.22146/ijc.79706

Abstract: *The adsorption of Cibacron Brilliant Yellow (CBY) 3-GP dye onto TiO_2 Degussa, Fe_2O_3, and TiO_2 anatase/Diphenylcarbizide in aqueous solution was studied with respect to temperature, contact time, and pH. The CBY 3-GP adsorption at equilibrium increased as the initial dye concentration increased for TiO_2/DPC, while it decreased for TiO_2 Degussa; however, it increased the initial dye concentration. The best removal efficiency was obtained at 1 mg for TiO_2/DPC, TiO_2 Degussa, and the amount of adsorption decreases with the rising of temperature. The negative $\Delta H°$ reveals the adsorption is exothermic and extremely negative $\Delta S°$ for TiO_2 Degussa. The negative value for $\Delta S°$ indicates a regular increase of the randomness at the TiO_2/DPC and Fe_2O_3 solution interface during adsorption. The intraparticle diffusion, pseudo-first- and second-order kinetic models were used. The Langmuir, Temkin, Freundlich, and Dubbin adsorption models were examined to describe the equilibrium isotherms. The usage of TiO_2 Degussa and TiO_2/DPC indicates that the equilibrium sorption was favorable.*

Keywords: *CBY dye; adsorption models; TiO_2 Degussa; Fe_2O_3; kinetic study; dynamic data*

■ INTRODUCTION

Due to their beneficial properties, such as strong interaction with the substrate, bright color, water-fastness, simple application techniques, and lower energy consumption required for the dying process, numerous highly reactive dyes, such as Cibacron Brilliant Yellow 3G-P (CBY) have been used in dyeing processes [1]. These characteristics reduce the water's clarity discharge since relatively small volumes of highly reactive dyes may result in ugly water discoloration and can have a very negative effect on waterways and biological systems. Therefore, the color removal from the effluents of the dye and textile industries is of great environmental significance. For the purpose of removing dye from wastewater effluents before release, a variety of wastewater treatment applications for processes such as chemical oxidation, coagulation, adsorption, filtering, and electrolysis have been made. The removal of colored materials, particularly dye, has been attempted using a variety of procedures that can be broadly categorized as physical, chemical, or biological treatment strategies, with varying degrees of success. The notable techniques are membrane separation, photodegradation, ozonation, adsorption, coagulation/flocculation, and biodegradation [2]. Because of its effectiveness, adsorption becomes one of the most well-known wastewater treatment techniques. Due to its operational importance in terms of technology, environment, and biology, adsorption is typically thought of as a significant separation process. Aqueous solutions, wastewater, and huge quantities of potable water are processed using a separation method that prioritizes the removal of low concentrations of contaminants [3].

One of the biggest threats to humanity is water contamination, which is linked to rapid industrialization and has generated a lot of research overall [4]. Due to their non-biodegradable characteristics, organic, and synthetic dyes—contaminant effluents removed from various food and textile industries—are one of the main sources of environmental contamination [5]. The most common method for removing dissolved organics from water is the adsorption process. For the removal of dye,

a variety of unconventional, affordable adsorbents has been tried. Peat-activated sludge, organic peel waste, tree fern [6], and minerals are a few of these. Additionally, the removal of color using activated carbon is made from unconventional sources such as sawdust, rice husk, and coir pith [7]. Therefore, it is essential to develop workable techniques to decrease the pollution brought on by Zn^{2+} discharges and to lower the dangers connected with its environmental presence. Industrial effluents can be treated in a variety of ways to remove heavy metal ions, which include ion exchange, solvent extraction, biodegradation, and adsorption [8]. Adsorption, however, is widely acknowledged as one of the most efficient methods for removing pollutants because of its low cost, ease of handling, low reagent usage, and potential for recovering value-added components through desorption and regeneration of adsorbent [9].

The most determinants of adsorption are greater adsorption ability implied by a larger surface area. The internal diffusion and mass transfer limitations to the penetration of the adsorbate into the adsorbent are decreased with smaller particle sizes (i.e., nearly complete adsorption capacity can be reached, and equilibrium is easier to achieve). The adsorption will be more thorough the longer the period of time.

Adsorption will be easier for substances with low solubility in water than for those with high solubility. Additionally, because non-polar compounds have a weaker affinity for water, they will be easier to remove than polar substances. The pH has an effect on a species' level of ionization. This then has an influence on adsorption.

Because the adsorbate molecules have higher vibrational energies and are, therefore, more likely to desorb from the surface, increasing the temperature generally reduces adsorption slightly. All of the applications that are relevant to us, however, take place in isothermal conditions. Various compounds that are particulate and have one dimension smaller than 100 nm in size make up the diverse class of materials known as nanoparticles (NPs) [10]. These materials can be 0D, 1D, 2D, or 3D, depending on the overall shape [11]. When researchers found that a substance's size could affect its physiochemical characteristics, such as its optical capabilities, they realized the significance of these materials. Semiconductor NPs have broad bandgaps, which led to a considerable change in their characteristics when the bandgap was tuned. Because of this, they are critical elements of photocatalysis, photo optics, and electronic devices. As an example, due to their optimal bandgap and band edge locations, a number of semiconductor NPs are discovered to be highly effective in water-splitting applications [12].

In this work, TiO_2 Degussa, Fe_2O_3, and TiO_2 anatase/Diphenylcarbizide (DPC) were used for the adsorption of CBY dye in an aqueous solution. The adsorption of CBY was first studied in a batch system by examining the effect of CBY concentration, contact time, and temperature, in several adsorption models Freundlich, Temkin, Dubbin, and Langmuir. Also, the kinetic data were evaluated in the adsorption process. Thermodynamic parameters were investigated that the adsorption of CBY on TiO_2 Degussa, TiO_2/DPC, and Fe_2O_3.

■ EXPERIMENTAL SECTION

Materials

The materials used in this study were ($C_{25}H_{15}Cl_3N_9Na_3O_{10}S_3$, Fig. 1) CBY 3G-P (Sigma Aldrich (USA), titanium(IV) *i*-propoxide (Ti(O*i*Pr)$_4$, 99.9% purity), Fe_2O_3, and TiO_2 Degussa were acquired from Sigma Aldrich (USA). Ethyl alcohol (EtOH Merck), DPC, HNO_3 (BDH. Co, LTD), sodium hydroxide NaOH (99% purity GCC, UK), and HCl (BDH) were purchased from other companies.

Instrumentation

The instrumentations used in this study were X-ray diffraction spectroscopy (D5000 XRD6000, Shimadzu, Japan), scanning electron microscopy (INSPECT S50 FEL, USA), atomic force microscopy (Sartorius Arium 611), and transmission electron microscopy TEM (Germany).

Procedure

Preparation of TiO_2/DPC

Ti(O*i*Pr)$_4$ in ethanol was used to dissolve TiO_2 before being mixed with distilled water at a molar ratio

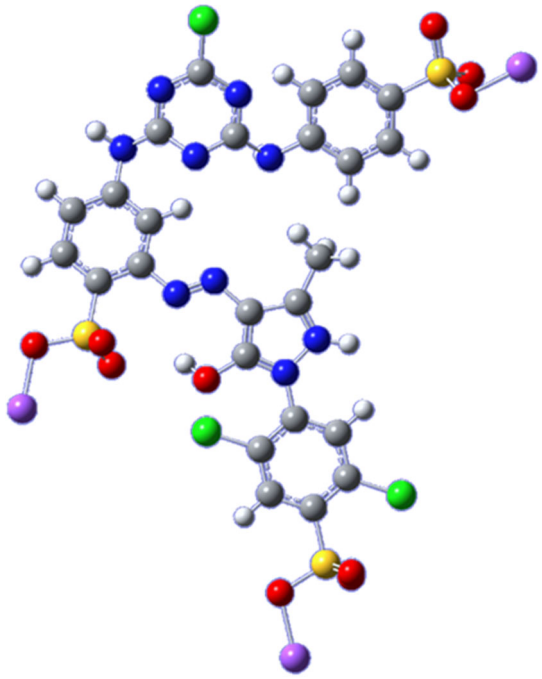

Fig 1. The chemical structure of CBY. Grey, white, blue, green, yellow, red, and purple color represent carbon, hydrogen, nitrogen, chlorine, sulfur, oxygen, and sodium atom, respectively

of TTIP:H_2O = 1:4 to produce the sol-gel TiO_2. HNO_3 was employed to change the pH and restrain the solution's hydrolysis process. The obtained solutions were stirred slowly and continuously for 40 min at room temperature. The gels were dried for 1.5 h at 500 °C to completely evaporate water and organic material in order to produce NPs [13]. Following ball milling [14], the resultant dry powders were subjected to a 2 h calcination process at 400 °C to produce TiO_2 nanocrystals. As for creating TiO_2/DPC, add 0.1 mol of DPC that has been dissolved in ethanol and 1.0 mol of the TiO_2 NPs solution that has been prepared previously. The mixture was stirred at room temperature for 30 min while it is separated by a centrifuge for 15 min, and then washed several times with water and ethanol to get rid of any extra residue. The material was taken, aged for 24 h, and then dried at 90 °C for 4 h before being stored for further analysis.

Adsorption experiments

The appropriate quantity (1 g) of CBY was dissolved in a liter of deionized water to create a stock solution at a concentration of 1 g/L. The stock solution was diluted with deionized water to create the working solutions, which were then given the proper concentration.

Erlenmeyer flasks containing 50 mL solution of 3G-P using TiO_2 Degussa, or TiO_2/DPC or Fe_2O_3 as adsorbent. The effect of various parameters, including solution pH 3–9, contact time 15–150 min, initial CBY concentration 2.18–10.9 mg/L, adsorbent dosage 1–5 mg, and temperature 15–90 °C was investigated. The pH of solutions was adjusted using 0.1 M HCl and/or 0.1 M NaOH. After each test, the adsorbent was separated from the aqueous solution, and the residual CBY in the aqueous solution was determined using absorption spectrometry. Double-beam UV-visible spectrophotometer was used to determine the concentrations of CBY dye in the solution. The concentration of the residual dye was measured at a maximum for the dye solution (428 nm) by taking samples at predetermined intervals, centrifuging them, and checking the supernatant for any remaining CBY. Based on a mass balance calculation, Eq. (1), the amount of adsorbed CBY (mg/g) was determined [15].

$$q_e = \frac{(C_0 - C_e)V}{M} \quad (1)$$

where C_e is the final or equilibrium concentration of CBY in the solution (mg/L), V is the volume of the solution (L), and W is the mass of TiO_2 Degussa, or TiO_2/DPC or Fe_2O_3 (g), q_e is the equilibrium adsorption capacity per gram weight of the adsorbent, and C_0 is the initial concentration of CBY in the solution (mg/L).

The flasks were shaken at 298 K for 2 h at a steady speed of 200 rpm. During the current investigation, the effects of factors such as the initial concentration and adsorbent dose were evaluated.

Effect of CBY initial concentration and contact time. The dye solutions were placed in an isothermal water bath shaker at initial concentrations of 2.18, 4.36, 6.55, 8.73, and 10.9 mg/L. For 24 h, the water bath shaker's temperature and rotational speed were set at 25 °C and 200 rpm, respectively.

Effect of temperatures. By varying the adsorption temperatures at 15, 30, 45, 60, 75, and 90 °C by adjusting the water bath shaker's temperature controller, the effect

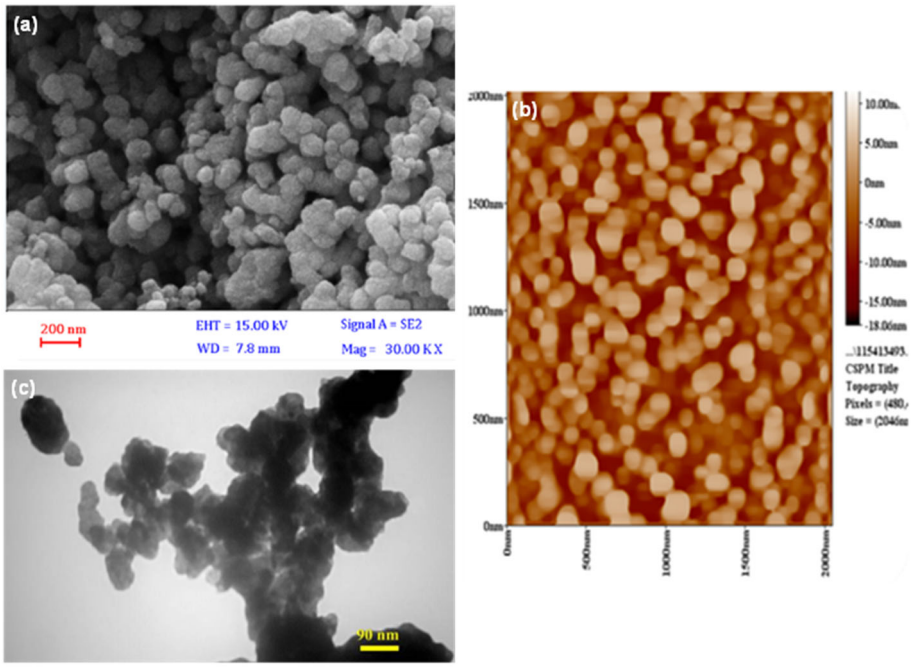

Fig 2. (a) SEM of TiO_2/DPC nanoparticle, (b) AFM of TiO_2/DPC nanoparticle, and (c) TEM of TiO_2/DPC nanoparticle

of temperatures on the adsorption process was investigated. The pH of the solution and other variables were left unchanged.

■ RESULTS AND DISCUSSION

Characterization of Adsorbents

The TiO_2 Degussa P25 crystallites are composed of 80% anatase and 20% rutile. Because of its inexpensive nature, great chemical stability, and reactivity, TiO_2 catalyst provides unique properties for a variety of environmental applications. Due to the wide surface area of the adsorption site, TiO_2 has good sorption properties. When there is a large concentration of hydroxyl groups (OH) on the surface of TiO_2, the contaminants can be adsorbed onto the material [16-17].

The group of iron-oxide minerals includes Fe_2O_3 crystals, which have a hexagonal shape and exhibit paramagnetic properties. Fe_2O_3 oxide can be activated under visible irradiation due to its small band gap (2.3 eV). Moreover, they have a powerful catalytic effect, are widely and simply accessible, and are incredibly ecologically friendly. Fe_2O_3 catalyst has the advantages of strong toxicity resistance and high catalytic activity [18].

Fig. 2(a) shows the SEM morphology images of TiO_2/DPC. The results indicate that the fine TiO_2/DPC has a spherical shape with dispersion nanoparticles the particle size of the TiO_2/DPC nanoparticle is 67 nm. The characteristic of TiO_2/DPC nanoparticles is determined by AFM as shown in Fig. 2(b), the particles size of TiO_2/DPC is 94.9 nm, while TEM images of sol-gel derived nanoparticles are shown in Fig. 2(c) is spherical and having diameter 37 nm. The band gap energy (Eg) of TiO_2/DPC is 2.1 eV which is smaller than the value of 3.2 eV for the bulk TiO_2.

Semiconductor NPs are materials that have properties that fall between those of metals and nonmetals. Substantial changes to their electrical and optical characteristics with a change in particle size. Due to their broad bandgaps, semiconductor NPs have demonstrated considerable changes in their characteristics when the bandgap is tuned. In light of this, they are finding use in photocatalysis, photo-optics, and electric devices [19].

Effect of Contact Time and Initial Concentration of Adsorbate

By varying the concentration of CBY solutions

between 2.18, 4.36, 6.55, 8.73, and 10.9 mg/L, it was possible to study the effect of increasing CBY concentrations on the adsorption onto TiO_2/DPC, TiO_2 Degussa, and Fe_2O_3 as shown in Fig 3. For TiO_2/DPC at 75 min, the CBY adsorption increased from 4.69 to 13.33 mg/g as the initial dye concentration increased from 1.6 to 9.17 mg/L. The results indicate that when CBY concentrations rise, so does the amount of adsorption, and they become constant. This occurs because the availability of CBY molecules at the interface rises with increased CBY concentration, which in turn improves the adsorption while decreasing from 2.25 to 0.078 mg/g for TiO_2 Degussa at 90 min. However, increased from 13 to 30.6 mg/g as the initial dye concentration. This phenomenon was due to an increase in the driving force of the concentration gradient as an increase in the initial dye concentration, then decreased to 2.3 mg/g for Fe_2O_3 at 60 min. Due to a large number of available surface sites, CBY was quickly adsorbed; however, as the process progressed toward equilibrium, it became difficult for CBY to interact with TiO_2 Degussa or Fe_2O_3 surface when all of the accessible sites were occupied, leading to saturated adsorption. Repulsion between the solute molecules and the bulk phases developed as a result of the difficulty in filling the remaining surface of sites [20].

Effect of pH

Adsorption isotherm of CBY onto TiO_2/DPC, TiO_2 Degussa, and Fe_2O_3 at different pH was recorded at pH 3 was more in compression pH at range 3, 4, 7, and 9. Since it was found that changing from an acidic to a basic medium's higher pH value considerably lowered the adsorption density of CBY. However, the adsorption increased with decreased pH to a value of around 3. As the pH is decreased, the positive charge on the surfaces of TiO_2/DPC and Fe_2O_3 increases. CBY is a non-ionic molecule that is easily adsorbed onto TiO_2/DPC, Fe_2O_3, and TiO_2 Degussa at a lower pH. The adsorption capabilities were greater in the acidic and neutral pH ranges and the lowest in the alkaline pH ranges. Whereas, at higher pH 9, Since the adsorbents are negatively charged, electrostatic repulsion reduces the rate of the sorption process. It is also understood that increasing pH results in an increase in hydroxyl ions, which reduces the adsorption capacities, the experimental data of the pH effect is in Table 1.

Effect of Adsorbent Weight

By using various concentrations of TiO_2/DPC, TiO_2 Degussa, and Fe_2O_3 ranging from 1 to 5 mg, q_e is CBY dye adsorbed amount on TiO_2/DPC, TiO_2 Degussa, and Fe_2O_3. The results showed in Table 2, in which the best-adsorbed amount was obtained at 1 mg for TiO_2/DPC and TiO_2 Degussa. The reason for this is that as the dosage of the adsorbent was increased, the adsorption

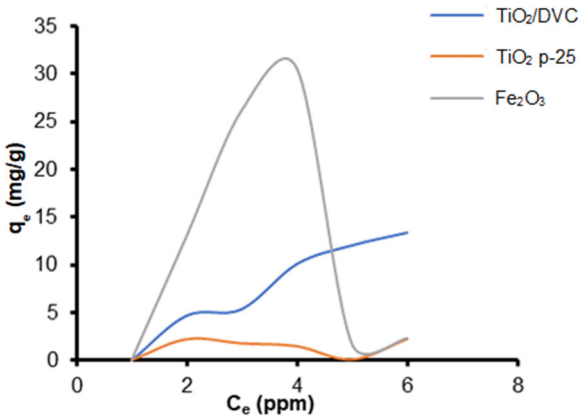

Fig 3. Adsorption effect of CBY solutions onto TiO_2/DPC, TiO_2 Degussa and Fe_2O_3

Table 1. Effect of solution pH on CBY adsorption (adsorbent TiO_2/DPC, TiO_2 Degussa, and Fe_2O_3), 75 min

Adsorbent	pH 3	pH 4	pH 7	pH 9
	q_e (mg/g)			
TiO_2 Degussa	6.06	3.98	8.18	0.90
TiO_2/DPC	0.63	0.56	0.46	0.46
Fe_2O_3	13.1	9.62	1.21	2.42

Table 2. Different quantities of TiO_2/DPC, TiO_2 Degussa, and Fe_2O_3 with the amount of adsorption

Weight (mg)	TiO_2/DPC	TiO_2 Degussa	Fe_2O_3
	q_e (mg/g)		
1	8.80	7.00	4.00
2	6.90	2.60	4.60
3	4.67	2.00	0.20
4	3.50	3.70	0.10
5	2.80	1.60	3.28

capability decreased, creating 2 mg of Fe_2O_3 the best-adsorbed amount. The interference and collision of active adsorbent sites at larger adsorbent dosages or the inability of the CBY dye in the solution to establish bonds with the accessible and active sites on the adsorbent to explain this result surfaces of TiO_2/DPC, TiO_2 Degussa, and Fe_2O_3 [21-22].

Effect Temperatures on CBY Adsorption

The results of a study of the effect of temperature on CBY adsorption at 15, 30, 45, 60, 75, and 90 °C can be used to indicate the exothermic nature of adsorption in detail. The increased tendency of the CBY to escape from the surface of TiO_2/DPC, TiO_2 Degussa, and Fe_2O_3 may be the cause of the decrease in adsorption as the temperature rises. Adsorption decreases when the temperature rises because the CBY's binding forces to the surface are reduced [23].

Increasing the temperature has improved the diffusion of dye molecules across the sample's exterior and internal boundary layers since it has reduced the viscosity of the solution [24]. Additionally, at higher temperatures, more dye molecules are mobile because they have more energy to interact with the adsorbent's active sites, allowing the dye to enter the pores of the adsorbent [25].

Effect of Temperature on Thermodynamic Parameters

From 15 to 55 °C, the influence of temperature on CBY adsorption on TiO_2/DPC, TiO_2 Degussa, and Fe_2O_3 (Fig 4) was studied. Eq. (2) and (3) can be used to get the Gibbs energy, G^0 (J/mol).

$$\Delta G^0 = \Delta H^0 - T\Delta S^0 \quad (2)$$

$$\Delta G^0 = -RT \ln K_c \quad (3)$$

The ability of the adsorbent to hold the adsorbate and the amount of mobility of the adsorbate within the solution are both represented by K_c, the equilibrium constant [26]. Eq. (4) or (5) can be used to determine the Kc, which is the ratio of the equilibrium concentration of the dye bound to the adsorbent to the equilibrium CBY concentration in solution (C_e) according to the Van't Hoff in Eq. (5) [27-28].

$$K_c = q_e / C_e \quad (4)$$

$$\ln K_c = \Delta S^0 / R - \Delta H^0 / RT \quad (5)$$

The slope and intercept of a linear plot between ln K_c and 1/T can be used to determine the values of ΔH^0 (J/mol) and ΔS^0 (J/mol K).

Thermodynamic parameters are shown in Table 3, with temperatures ranging from 15 to 55 °C. The possibility of the process and the spontaneous nature of the adsorption are indicated by the negative value of G^0 at various temperatures. Usually, the enthalpy of adsorption changes. The exothermic and physical nature of the adsorption is indicated by the negative ΔH^0 (-29074.0 J/mol). Additionally, the CBY adsorption process' slightly negative ΔS^0 indicates a regular rise in

Table 3. Thermodynamic parameters of CBY adsorption onto TiO_2 Degussa, TiO_2/DPC, and Fe_2O_3

Materials	ΔH (J/mol)	ΔS (J/mol K)	ΔG (J/mol)
TiO_2(P25)	-29074.0	-56.2	-11762.2
TiO_2/DPC	34503.1	-21.3	41058.3
Fe_2O_3	75054.6	-25.9	83054.3

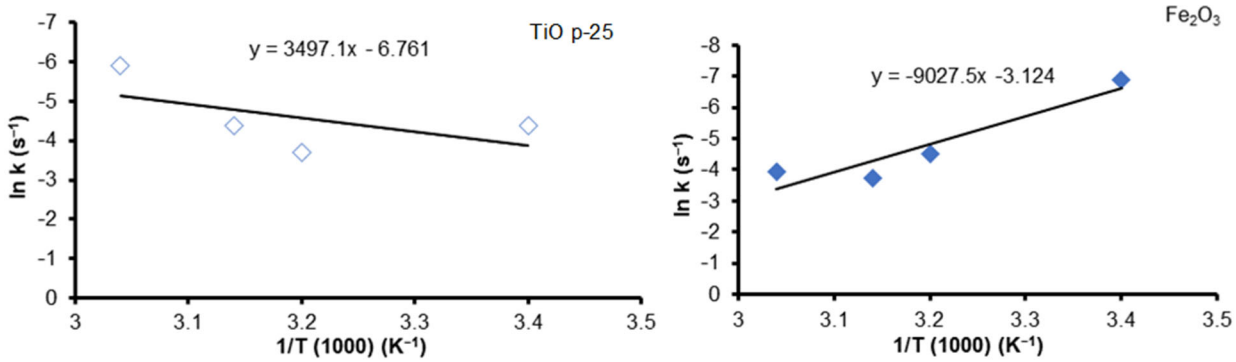

Fig 4. Effect of temperature on CBY adsorption onto TiO_2 Degussa, Fe_2O_3

the randomness at the TiO_2(P25) solution interface throughout adsorption. State exothermic adsorption of CBY and reduced randomness at the boundary layer between TiO_2(P25) and aqueous solution, indicating exothermic adsorption of CBY on the adsorbent and destroyed active sites of TiO_2(P25) surface.

Table 3 also displays the rising temperature, as shown by the positive value of ΔG^0 at various temperatures. Usually, the variation of the adsorption enthalpy.

The positive ΔH^0 (34503.1 and 75054.6 J/mol) indicates that the adsorption is chemical in nature and endothermic. Additionally, the CBY adsorption process' slightly negative ΔS^0 value shows a consistent rise in randomness at the interface of the TiO_2/DPC or Fe_2O_3 solution during adsorption. This suggests that the CBY dye was adsorbed in this condition by an endothermic process.

At higher temperatures for dye, the surface coverage increased. This can be related to the development of additional active sites or the enhanced penetration of reactive dyes into microspores at higher temperatures. Several publications have observed endothermic adsorption of reactive dyes on various types of adsorbents, resulting in the creation of more than one molecular layer on the surface of TiO_2/DPC [29].

The following isotherms were used to fit the data: Freundlich, Temkin, and Langmuir [30].

Langmuir adsorption isotherm

The model presupposes homogeneous adsorption energies on the surface and a lack of adsorptive transmigration in the surface plane. These suppositions led Langmuir to represent Eq. (6) and (7):

$$\frac{1}{q_e}=\frac{1}{q_0}+\frac{1}{q_0 K_L q_e} \quad (6)$$

$$C_e/q_e = 1/q_{max}\, K_L + C_e/q_{max} \quad (7)$$

where q_0 is the highest monolayer coverage capacity (mg/g), K_L = Langmuir isotherm constant (L/mg), C_e is the adsorbate's equilibrium concentration (mg/L), and q_e = the number of substances adsorbent at equilibrium (mg/g).

The values of q_{max} and K_L were calculated using the slope and intercept of the Langmuir plot of $1/q_e$ vs $1/C_e$ and R_L, the separation factor (also known as the equilibrium parameter), which is a dimensionless constant.

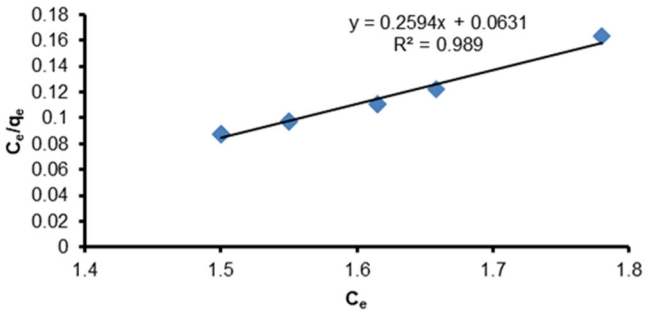

Fig 5. Linear Langmuir adsorption isotherm TiO_2 Degussa

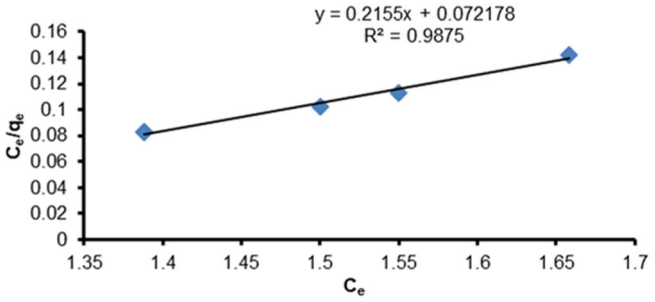

Fig 6. Linear Langmuir adsorption isotherm TiO_2/DPC

$$RL=\frac{1}{1+\left(1+K_L C_e\right)} \quad (8)$$

where K_L is a constant relating to adsorption energy (Langmuir Constant), initial concentration C_0, and R_L value indicates whether the adsorption is favorable or unfavorable. The estimated data show that the Langmuir isotherm is favorable since the RL is larger than 0 but less than 1 according to the data. The K_L from this research work is 4.1109, and 2.9855 L/mg, as RL values are 0.10038, and 0.0520 for TiO_2 Degussa, and TiO_2/DPC indicating that the equilibrium sorption was favorable. When it comes to Fe_2O_3, Langmuir adsorption is not applicable.

Fig. 5 and 6 display a linear Langmuir adsorption isotherm. The slope and intercept of the linear plot of C_e/q_e vs C_e were used to compute the values of q_m and K_L of the Langmuir adsorption isotherm, indicating that it is the Langmuir equation for TiO_2 Degussa that best fits the experimental data.

Freundlich adsorption isotherm

These data often fit the empirical equation proposed by Freundlich (Eq. (9)),

$$\ln q_e = \ln K_f + 1/n \ln C_e \quad (9)$$

where K_f = Freundlich isotherm constant (mg/L), q_e = the number of materials adsorbed per gram of adsorbent at equilibrium (mg/g), n is the adsorption intensity, and C_e is the equilibrium adsorbate concentration (mg/L). While 1/n is a function of the strength of adsorption in the adsorption process, the constant K_f is a rough indicator of adsorption capacity. The value of 1/n is below one for TiO_2 Degussa, and TiO_2/DPC and Fe_2O_3 it indicates normal adsorption. The constants k and n change with temperature in order to account for the empirical finding that the quantity adsorbed rises more slowly is needed to saturate the surface. While the sorbent-sorbate system's K_f and n properties must be determined by data fitting, the smaller 1/n, the greater the expected heterogeneity, even though linear regression is commonly employed to create the parameters of kinetic and isotherm models. An isotherm of linear adsorption results from this expression.

Temkin isotherm

This isotherm has a component that explicitly accounts for the interactions between the adsorbent and adsorbate. By neglecting the extremely low and high concentration values, the model assumes that the heat of adsorption of all molecules in the layer will decrease linearly rather than logarithmically with coverage. By graphing the amount sorbed q_e versus ln C_e and calculating the constants from the slope and intercept, it was possible to demonstrate that, as predicted by the equation, the derivation is characterized by a uniform distribution of binding energies. Eq. (10) and (11) provide the model.

$$B = RT/b_T \quad (10)$$

$$q_e = B\ln A_T + B\ln C_e \quad (11)$$

where T = temperature at 298 K, A_T = Temkin isotherm equilibrium binding constant (L/g), R = universal gas constant (8.314J/mol/K), bT = Temkin isotherm constant, and B = heat of sorption constant (J/mol). The following values, which are a measure of the heat of sorption and indicate a physical adsorption process, are taken from the Temkin plot in Fig. 7, 8, and 9 [31].

Dubinin–Radushkevich isotherm model

On a heterogeneous surface, the Dubinin-Radushkevich isotherm is typically used to express the adsorption mechanism [32]. The results from the intermediate range of concentrations and high solute activity have generally been well fit by the model (Eq. (12)).

$$\ln q_e = \ln q_s - K_{ad}\varepsilon^2 \quad (12)$$

where are q_e = amount of adsorbate in the adsorbent at equilibrium (mg/g), K_{ad} = Dubinin–Radushkevich isotherm constant (mol^2/kJ^2), and q_s = theoretical isotherm saturation capacity (mg/g). The method was typically used to differentiate between the physical and chemical adsorption of metal ions with its mean free energy, ε per molecule of adsorbate, which can be calculated by the relationship (Eq. (13)).

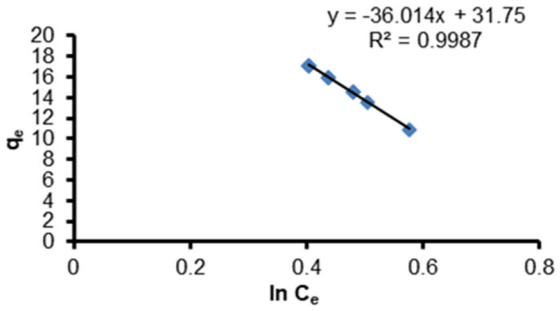

Fig 7. Temkin adsorption isotherm using TiO_2 Degussa

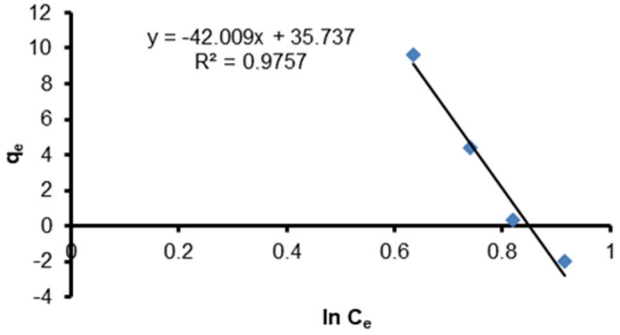

Fig 8. Temkin adsorption isotherm using Fe_2O_3

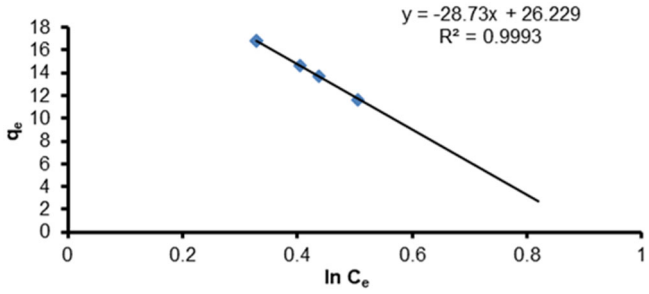

Fig 9. Temkin adsorption isotherm using TiO_2/DPC

$$\varepsilon = RT\ln\left(1+1/C_e\right) \quad (13)$$

where R, T, and C_e stand for the equilibrium adsorbate concentrations(mg/L), the gas constant in J/mol K, and the absolute temperature (K), respectively. When adsorption data at various temperatures are represented as a function of the logarithm of quantity adsorbed ($\ln q_e$) vs. ε^2 the square of potential energy, the Dubinin-Radushkevich isotherm model's temperature dependence is one of the model's distinct features. The characteristic curve is also known as the curve on which all acceptable data will lie [33]. Eq. (13) was used to determine constants like q_s and K_{ad} from Fig. 10, 11, and 12. From the linear plot of the Dubinin-Radushkevich model, q_s was determined to be 1.436 mg/g, K_{ad} was determined 3×10^{-7} the $R^2 = 0.997$ for TiO_2/DPC, while Fe_2O_3 and TiO_2 Degussa do not apply (Table 4).

The results of isotherm parameters (Langmuir, Freundlich, Temkin, and Dubinin-Radushkevich) applied in this study for the following in Table 5.

The parameter results in Table 5 Langmuir model using TiO2/DPC, TiO_2 Degussa, and Fe_2O_3. The active site can only adsorb one molecule, thus the K_L value for all adsorption systems displays a relatively low value, indicating weak interaction between the molecules of the absorbent and adsorbate. TiO_2/DPC and TiO_2 Degussa have relatively high correlation values ($R^2 > 0.80$) than Fe_2O_3.

Table 5 displays the parameters of the Freundlich model when TiO_2/DPC, TiO_2 Degussa, and Fe_2O_3 adsorbents. Freundlich isotherm is a good representation of TiO_2/DPC and TiO_2 Degussa P25 adsorption systems than the Fe_2O_3 adsorption system; this is confirmed by the R^2 value of higher than 0.80, the adsorption process takes place on a heterogeneous surface in a multilayer form with weak interactions between the adsorbent and adsorbate.

The parameter results from the Temkin model using TiO_2/DPC, TiO_2 Degussa, and Fe_2O_3. A comparatively low value between the molecules of the absorbent and the adsorbate is shown by the AT value for all adsorption systems. Physical interaction only involves more interaction weak, correlation coefficient value ($R^2 > 0.80$), for TiO_2/DPC, TiO_2 Degussa, and Fe_2O_3 are suitable with Temkin isotherm.

While results Dubinin-Radushkevich model using TiO_2/DPC, TiO_2 Degussa, and Fe_2O_3 have small β values. Influenced by pore volume for β value. The highest maximal binding energy value is impacted by the greater pore volume. TiO_2/DPC, TiO_2 Degussa adsorption system, and TiO_2 have the best correlation coefficient values ($R^2 > 0.80$), indicating that they have the greatest

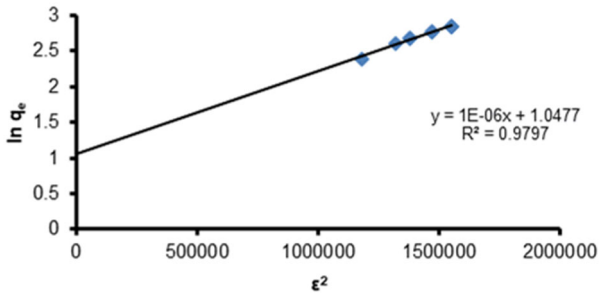

Fig 10. Dubinin-Radushkevich adsorption isotherm using TiO_2 Degussa

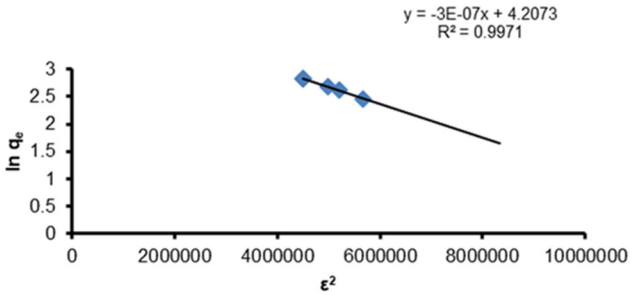

Fig 11. Dubinin-Radushkevich adsorption isotherm using TiO_2/DPC

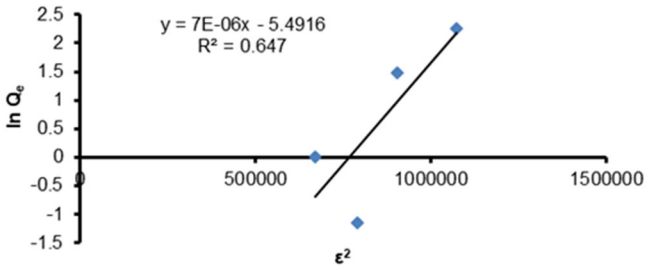

Fig 12. Dubinin-Radushkevich adsorption isotherm using Fe_2O_3

Table 4. Dubinin-Radushkevich adsorption isotherm constants

Material	K_{ad}	q_s	R^2
TiO_2/DPC	3×10^{-7}	1.436	0.997
TiO_2 Degussa	-1×10^{-6}	2.851	0.979
Fe_2O_3	-7×10^{-6}	4.120×10^{-3}	0.647

Table 5. Isotherm parameters (Langmuir, Temkin, Freundlich, and Dubinin-Radushkevich)

Langmuir isotherm parameters				
Adsorbent	K_L (L/mg)	RL	R^2	Note
TiO_2/DPC	2.9850	0.05200	0.987	0 < RL < 1 favorable adsorption
TiO_2 Degussa	4.1109	0.10038	0.978	R^2 > 0.80, monolayer adsorption
Fe_2O_3	–0.4920	1.0000	0.407	Linear adsorption process, RL = 1. (Depending on the amount adsorbed and the concentration adsorbed) R^2 < 0.80 does not suggest monolayer adsorption
Freundlich isotherm parameters				
Adsorbent	1/n	n	R^2	Note
TiO_2/DPC	–2.014	–0.496	0.993	n < 1, chemical interaction between adsorbate molecules R^2 > 0.80, multilayer adsorption
TiO_2 Degussa	–2.557	–0.390	0.988	
Fe_2O_3	–9.960	–0.100	0.615	
Temkin isotherm parameters				
Adsorbent	A_T (L/g)	B_T (J/mol)	R^2	Note
TiO_2/DPC	0.334	–83.304	0.993	B_T < 8 kJ/mol, physical interaction between adsorbate molecules
TiO_2 Degussa	0.414	–66.486	0.998	R^2 > 0.80, uniform distribution adsorbate to the adsorbent surface
Fe_2O_3	0.427	–56.998	0.979	
Dubinin-Radushkevich isotherm parameters				
Adsorbent	B (mol^2/kJ^2)	E (kJ/mol)	R^2	Note
TiO_2/DPC	0.3×10^{-6}	1291.088	0.997	E > 8 kJ/mol, chemical interaction between adsorbate molecules
TiO_2Degussa	1×10^{-6}	707.107	0.979	R^2 > 0.80, micro pore size is existing in the adsorbent surface
Fe_2O_3	7×10^{-6}	267.265	0.647	

correlation coefficient, while Fe_2O_3 has the correlation coefficient is low ($R^2 = 0.647$). Temkin model was discovered to have the best fit because it had the greatest regression value.

Kinetic of sorption

Kinetic models have been used to analyze the mechanism of sorption and potential rate-controlling processes in order to select the appropriate operating parameters for full-scale batch operation [34]. The models utilized were pseudo-first-order, pseudo-second-order, and zeroth-order kinetic models.

Pseudo-first-order model. The -first-order rate expression based on solid capacity is generally expressed as follows Eq. (14) and (15):

$$\ln(q_e - q_t) = \ln q_e - k_1 t \quad (14)$$

$$\ln(C_0 - C_t) = \ln C_0 kt \quad (15)$$

where q_t is the amount adsorbed at time t (mg/g), C_t is the concentration at the time, q_e is the amount of CBY adsorbed at equilibrium (mg/g), k_1 is the rate constant of first-order adsorption (1/min), and C_o is the initial concentration. From the ln (q_e – q_t) against t straight-line plot, the value of the adsorption rate constant k_1 for the CBY adsorption onto (TiO_2 Degussa, TiO_2/DPC, or Fe_2O_3) was calculated (Fig. 13, 14, and 15). The data were fitted with correlation coefficients, showing that the first-order equation is followed by the rate of removal of CBY.

The findings were poorly correlated, showing that the rate of removal of CBY onto TiO_2 Degussa, TiO_2/DPC, or Fe_2O_3 is not followed by the second-order equation.

Pseudo-second-order model. With the use of the following Eq (16), the second-order kinetic rate was investigated.

$$\frac{t}{C_t} = \frac{1}{k_2 q_e^2} + \frac{1}{qe} \quad (16)$$

where k_2, C_t, and q_e stand for the rate constant, the concentration at a given time 't' and the amount adsorbed at equilibrium, respectively. By displaying the

graph of t/C_t versus t, With the use of the following equation, the second-order kinetic rate was investigated. The value of $k_2 = 1.06 \times 10^{-5}$ g/mg min, $q_e = 416.66$ mg/g and $R^2 = 0.4138$ for TiO_2/DPC (Fig. 16); $k_2 = 0.0618 \times 10^{-5}$ g/mg min, $Q_e = 1666.66$ mg/g, and $R^2 = 0.5728$ for TiO_2 Degussa (Fig. 18); and $K_2 = 0.24 \times 10^{-5}$ g/mg min, $Q_e = 1000$ mg/g, and $R^2 = 0.2134$ for Fe_2O_3 (Fig. 17) were calculated. The CBY adsorption onto TiO_2 Degussa, TiO_2/DPC, and Fe_2O_3 was in loose agreement with the total rate of CBY adsorption on to TiO_2 Degussa, TiO_2/DPC, and Fe_2O_3, according to the obtained kinetic adsorption data, which appeared to be controlled by the physicochemical process.

The pseudo-first-order model, which is often relevant over the first stage of an adsorption process, is predicated on the idea that the rate of change in solute uptake with time is perfectly proportional to the difference in saturation concentration and the amount of solid uptake with time. When adsorption occurs through diffusion through the interface, it is usually seen that kinetics follows this pseudo-first-order rate equation, and the intercept of ln ($q_e - q_t$) vs t plots would therefore be equal to ln of empirically obtained q_e to fit the experimental value, the pseudo-first-order equation usually does not provide a good fit over the entire range of adsorption time.

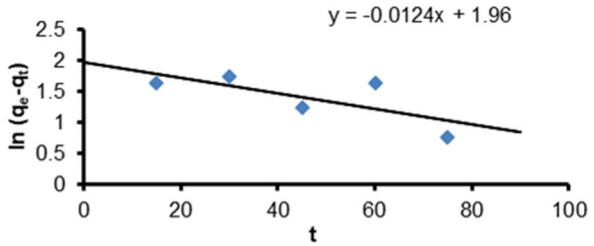

Fig 13. Pseudo-first-order of CBY adsorption onto TiO_2 Degussa

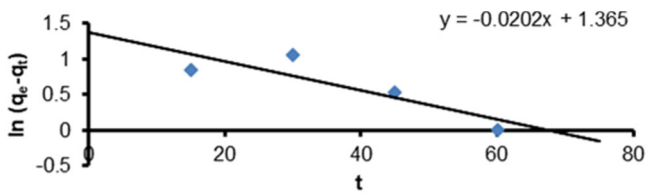

Fig 14. Pseudo-first-order of CBY adsorption onto TiO_2/DPC

The pseudo-second-order kinetic model predicts behavior over the whole adsorption range under the assumption that chemisorption is the rate-limiting step;

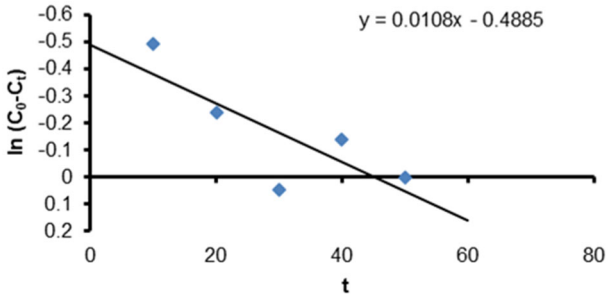

Fig 15. Pseudo-first-order of CBY adsorption onto Fe_2O_3

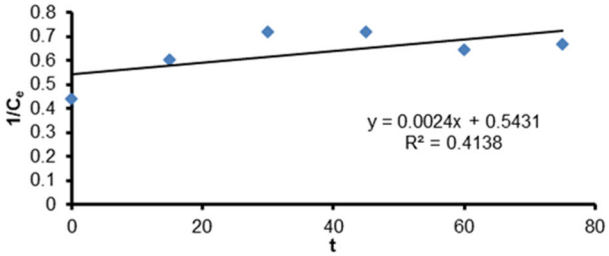

Fig 16. Pseudo-second-order of CBY adsorption onto TiO_2/DPC

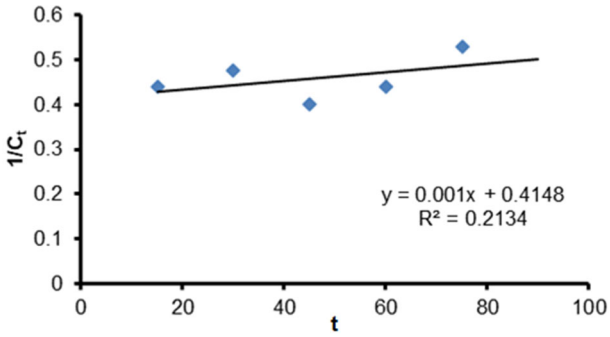

Fig 17. Pseudo-second-order of CBY adsorption onto Fe_2O_3

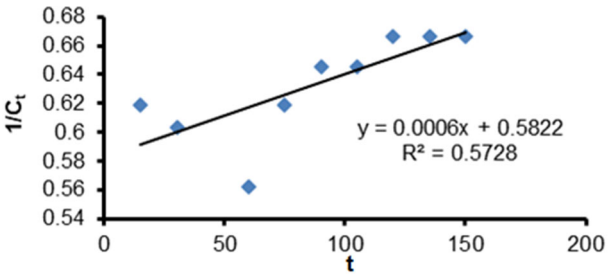

Fig 18. Pseudo-second-order of CBY adsorption onto TiO_2 Degussa

Table 6. Rate constants and correlation coefficients for models studied of the kinetic equations

Adsorbents	Pseudo-zeroth-order		Pseudo-first-order		Pseudo-second-order	
	K (mg g/min)	R^2	K_1 (1/min)	R^2	K_2 (g/mg min) × 10^{-5}	R^2
TiO_2/DPC	0.434	0.452	0.0202	0.817	1.060	0.413
TiO_2 Degussa	0.904	0.357	0.0124	0.737	0.062	0.573
Fe_2O_3	-0.711	0.163	0.0108	0.634	0.213	0.213

the adsorption rate is determined by adsorption capacity rather than adsorbate concentration. This model has several advantages over the Lagergren first-order model, one of which is the ability to compute the equilibrium adsorption capacity.

According to studies, values of $R^2 > 0.8$ show a strong fit between the data and the model, while values of $R^2 < 0.5$ indicate a weak correlation between the predictor variable and the response variable, based on Table 6, it is expected that is suitable for pseudo-first-order according to the values of R^2.

■ CONCLUSION

Adsorption was influenced by some operational factors, including temperature, initial concentration, pH, and contact time. The study of the CBY dye's adsorption to the TiO_2/DPC, TiO_2 Degussa, and Fe_2O_3 materials revealed that as the concentration of CBY increases, more CBY molecules are available at the interface, which improves the adsorption. It can be inferred that electrostatic repulsion plays a significant role in this system, given that the amount of adsorption increases with increasing CBY concentration. This was caused by an increase in initial dye concentration reducing pH, which increased the driving force of the concentration gradient. The increased tendency of the CBY to escape from the surfaces of TiO_2/DPC, TiO_2 Degussa, and Fe_2O_3 may be the cause of the decrease in adsorption as the temperature rises. Demonstrate the viability of the procedure and the spontaneous nature of the adsorption at various temperatures. The CBY adsorption process' negative result for ΔS^0 implies a regular rise in randomness at the interface of the adsorbent throughout adsorption. The TiO_2 Degussa Langmuir equation provides the experimental data with the best match compared to the other isotherm. The CBY adsorption onto the adsorbent surfaces was confirmed by the obtained kinetic adsorption data, proving that the pseudo-first-order equation is really followed by the rate of CBY removal from these surfaces. The study's findings were well-explained by Freundlich, Langmuir, Temkin, and Dubbin-Radushkevich. The experimental results had the best fit with the Langmuir equation. The kinetic data showed that a pseudo-first-order equation was in control of the adsorption process. Thermodynamic investigations showed that the adsorption of CBY on the adsorbent was both endothermic and chemical in nature, as well as exothermic and occurring spontaneously.

■ REFERENCES

[1] Khan, T.A., Singh, V.V., and Kumar, D., 2004, Removal of some basic dyes from artificial textile wastewater by adsorption on Akash Kinari coal, *J. Sci. Ind. Res.*, 63 (4), 355–364.

[2] Khamparia, S., and Jaspal, D.K., 2017, Adsorption in combination with ozonation for the treatment of textile waste water: A critical review, *Front. Environ. Sci. Eng.*, 11 (1), 8.

[3] Nwodika, C., and Onukwuli, O.D., 2017, Adsorption study of kinetics and equilibrium of basic dye on kola nut pod carbon, *Gazi Univ. J. Sci.*, 30 (4), 86–102.

[4] Shahabuddin, S., Khanam, R., Khalid, M., Sarih, N.M., Ching, J.J., Mohamad, S., and Saidur, R., 2018, Synthesis of 2D boron nitride doped polyaniline hybrid nanocomposites for photocatalytic degradation of carcinogenic dyes from aqueous solution, *Arabian J. Chem.*, 11, 1000–1016.

[5] Zhou, X., Zheng, P., Wang, L., and Liu, X., 2019, Preparation of sulfonated poly(arylene ether

nitrile)-based adsorbent as a highly selective and efficient adsorbent for cationic dyes, *Polymers*, 11 (1), 32.

[6] Onur, I., Demir, I., Yuceer, A., and Cinar, O., 2017, Isotherm and kinetic modelling of azo dyes adsorption, *Eur. J. Eng. Nat. Sci.*, 2 (1), 210–216.

[7] Malik P.K., 2003, Use of activated carbons prepared from sawdust and rice-husk for adsorption of acid dyes: A case study of Acid Yellow 36, *Dyes Pigm.*, 56 (3), 239–249.

[8] Qasem, N.A.A., Mohammed, R.H., and Lawal, D.U., 2021, Removal of heavy metal ions from wastewater: A comprehensive and critical review, *npj Clean Water*, 4 (1), 36.

[9] Baskar, A.V., Bolan, N., Hoang, S.A., Sooriyakumar, P., Kumar, M., Singh, L., Jasemizad, T., Padhye, L.P., Singh, G., Vinu, A., Sarkar, B., Kirkham, M.B., Rinklebe, J., Wang, S., Wang, H., Balasubramanian, R., and Siddique, K.H.M., 2022, Recovery, regeneration and sustainable management of spent adsorbents from wastewater treatment streams: A review, *Sci. Total Environ.*, 822, 153555.

[10] Joudeh, N., and Linke, D., 2022, Nanoparticle classification, physicochemical properties, characterization, and applications: A comprehensive review for biologists, *J. Nanobiotechnol.*, 20 (1), 262.

[11] Byakodi, M., Shrikrishna, N.S., Sharma, R., Bhansali, S., Mishra, Y., Kaushik, A., and Gandhi, S., 2022, Emerging 0D, 1D, 2D, and 3D nanostructures for efficient point-of-care biosensing, *Biosens. Bioelectron.: X*, 12, 100284.

[12] Hisatomi, T., Kubota, J., and Domen, K., 2014, Recent advances in semiconductors for photocatalytic and photoelectrochemical water splitting, *Chem. Soc. Rev.*, 43 (22), 7520–7535.

[13] Bokov, D., Turki Jalil, A., Chupradit, S., Suksatan, W., Javed Ansari, M., Shewael, I.H., Valiev, G.H., and Kianfar, E., 2021, Nanomaterial by sol-gel method: Synthesis and application, *Adv. Mater. Sci. Eng.*, 2021, 5102014.

[14] Thangavelu, K., Annamalai, R., and Arulnandhi, D., 2013, Preparation and characterization of nanosized TiO_2 powder by sol-gel precipitation route, *Int. J. Emerging Technol. Adv. Eng.*, 3 (1), 636–639.

[15] Ahmad, M.A., Herawan, S.G., and Yusof, A.A., 2014, Equilibrium, kinetics, and thermodynamics of remazol brilliant blue R dye adsorption onto activated carbon prepared from pinang frond, *Int. Scholarly Res. Not.*, 2014, 184265.

[16] Xiao, G., Su, H., and Tan, T., 2015, Synthesis of core–shell bioaffinity chitosan–TiO_2 composite and its environmental applications, *J. Hazard. Mater.*, 283, 888–896.

[17] El Mouchtari, E.M., Daou, C., Rafqah, S., Najjar, F., Anane, H., Piram, A., Hamade, A., Briche, S., and Wong-Wah-Chung, P., 2020, TiO_2 and activated carbon of *Argania spinosa* tree nutshells composites for the adsorption photocatalysis removal of pharmaceuticals from aqueous solution, *J. Photochem. Photobiol., A*, 388, 112183.

[18] Wang, N., Ye, C., Xie, H., Yang, C., Zhou, J., and Ge, C., 2021, Fe_2O_3 enhanced high-temperature arsenic resistance of CeO_2–La_2O_3/TiO_2 catalyst for selective catalytic reduction of NOx with NH_3, *RSC Adv.*, 11 (16), 9395–9402.

[19] Tiwari, A.P., and Rohiwal, S.S., 2019, "Synthesis and Bioconjugation of Hybrid Nanostructures for Biomedical Applications" in *Hybrid Nanostructures for Cancer Theranostics*, Eds. Ashok Bohara, R., and Thorat, N., Elsevier, Amsterdam, Netherlands, 17–41.

[20] Ahmad, M.A., and Alrozi, R., 2011, Removal of malachite green dye from aqueous solution using rambutan peel-based activated carbon: Equilibrium, kinetic and thermodynamic studies, *Chem. Eng. J.*, 171 (2), 510–516.

[21] Fan, T., Liu, Y., Feng, B., Zeng, G., Yang, C., Zhou, M., Zhou, H., Tan, Z., and Wang, X., 2008, Biosorption of cadmium(II), zinc(II) and lead(II) by *Penicillium simplicissimum*: Isotherms, kinetics and thermodynamics, *J. Hazard. Mater.*, 160 (2-3), 655–661.

[22] Tamjidi, S., and Esmaeili, H., 2019, Chemically modified CaO/Fe_3O_4 nanocomposite by sodium

dodecyl sulfate for Cr(III) removal from water, *Chem. Eng. Technol.*, 42 (3), 607–616.

[23] Singh, K., Kumar, A., Awasthi, S., Pandey, S.K., and Mishra, P., 2019, Adsorption mechanism of carboxymethyl cellulose onto mesoporous mustard carbon: Experimental and theoretical aspects, *Colloids Surf., A*, 581, 123786.

[24] Alkan, M., Doğan, M., Turhan, Y., Demirbaş, Ö., and Turan, P., 2008, Adsorption kinetics and mechanism of maxilon blue 5G dye on sepiolite from aqueous solutions, *Chem. Eng. J.*, 139 (2), 213–223.

[25] Zghal, S., Jedidi, I., Cretin, M., Cerneaux, S., and Abdelmouleh, M., 2023, Adsorptive removal of Rhodamine B dye using carbon graphite/CNT composites as adsorbents: Kinetics, isotherms and thermodynamic study, *Materials*, 16 (3), 1015.

[26] Banerjee, S., and Chattopadhyaya, M.C., 2017, Adsorption characteristics for the removal of a toxic dye, tartrazine from aqueous solutions by a low cost agricultural by-product, *Arabian J. Chem.*, 10 (Suppl. 2), S1629–S1638.

[27] Bhattacharyya, K.G., and Sarma, A., 2003, Adsorption characteristics of the dye, Brilliant Green, on Neem leaf powder, *Dyes Pigm.*, 57 (3), 211–222.

[28] Aljeboree, A.M., Alshirifi, A.N., and Alkaim, A.F., 2017, Kinetics and equilibrium study for the adsorption of textile dyes on coconut shell activated carbon, *Arabian J. Chem.*, 10, S3381–S3393.

[29] Abdoul, H.J., Yi, M., Prieto, M., Yue, H., Ellis, G.J., Clark, J.H., Budarin, V.L., and Shuttleworth, P.S., 2023, Efficient adsorption of bulky reactive dyes from water using sustainably-derived mesoporous carbons, *Environ. Res.*, 221, 115254.

[30] Habeeb, O.A., Ramesh, K., Ali, G.A.M., Yunus, R.M., and Olalere, O.A., 2017, Kinetic, isotherm and equilibrium study of adsorption capacity of hydrogen sulfide-wastewater system using modified eggshells, *IIUM Eng. J.*, 18 (1), 13–25.

[31] Inyinbor, A.A., Adekola, F.A., and Olatunji, G.A., 2016, Kinetics, isotherms and thermodynamic modeling of liquid phase adsorption of Rhodamine B dye onto *Raphia hookerie* fruit epicarp, *Water Resour. Ind.*, 15, 14–27.

[32] Hu, Q., and Zhang, Z., 2019, Application of Dubinin–Radushkevich isotherm model at the solid/solution interface: A theoretical analysis, *J. Mol. Liq.*, 277, 646–648.

[33] Foo, K.Y., and Hameed, B.H., 2010, Insights into the modeling of adsorption isotherm systems, *Chem. Eng. J.*, 156 (1), 2–10.

[34] Cáceres-Jensen, L., Rodríguez-Becerra, J., Garrido, C., Escudey, M., Barrientos, L., Parra-Rivero, J., Domínguez-Vera, V., and Loch-Arellano, B., 2021, Study of sorption kinetics and sorption–desorption models to assess the transport mechanisms of 2,4-dichlorophenoxyacetic acid on volcanic soils, *Int. J. Environ. Res. Public Health*, 18 (12), 6264.